RSC Advances

PAPER

View Article Online
View Journal | View Issue

Cite this: *RSC Adv.*, 2017, **7**, 27863

Synthesis and characterization of some nanostructured composite oxides for low temperature catalytic combustion of dilute propane

C. Doroftei *[a] and L. Leontie[ab]

Received 6th April 2017
Accepted 22nd May 2017

DOI: 10.1039/c7ra03916f

rsc.li/rsc-advances

Powders of five nanosized perovskites, $SrMnO_3$, $SrCoO_3$, $GdAlO_3$, $FeMnO_3$, $La_{0.6}Pb_{0.2}Mg_{0.2}MnO_3$, and four ferrospinels, $MgFe_2O_4$, $Ni_{0.5}Co_{0.5}Fe_2O_4$, $Ni_{0.5}Co_{0.5}Fe_{1.9}Sc_{0.1}O_4$, $Ni_{0.5}Co_{0.5}Fe_{1.8}Sc_{0.2}O_4$, were prepared by a sol–gel self-combustion technique. The powders were catalytically tested in the flameless combustion of dilute propane at atmospheric pressure. All samples had nanocrystalline structures and the crystallite sizes were in the range of 26–89 nm. Catalytic testing showed a significant dependence of the catalytic performance on the catalyst composition. As experiments revealed, the $La_{0.6}Pb_{0.2}Mg_{0.2}MnO_3$ perovskite catalyst, with a specific surface area of 8.6 $m^2\ g^{-1}$, exhibits the best performance in propane conversion, of about 92% at 350 °C. The lowest catalytic efficiency was obtained for $FeMnO_3$ and $SrCoO_3$ catalysts. Different reactivities of active oxygen species involved in the catalytic oxidation reaction determine registered differences in catalytic activity of oxide compounds. The results suggest that the $La_{0.6}Pb_{0.2}Mg_{0.2}MnO_3$ perovskite can be a suitable catalyst for catalytic combustion of dilute propane at low temperatures (below 400 °C).

1. Introduction

The progressive increase of volatile organic compound (VOC) emissions requires the development of new technologies for their removal from the atmosphere.[1–3] Compared to conventional thermal incineration, catalytic combustion is considered a far more efficient method for removing low concentrations of VOCs from gaseous streams.[2,4] Catalytic combustion is also more economical because it can operate at low temperatures (<500 °C) with diluted effluent streams (<1% VOC). Catalytic combustion performance is strongly dependent on the type of catalyst used. Two categories of catalysts have been typically employed for VOC oxidation reactions: noble metals and transition metal oxides.[5–11] Noble metal catalysts display, in general, high hydrocarbon combustion activity, but they are expensive and more prone to deactivation by poisoning. The transition metal oxide catalysts are, generally, less active than noble metals, but more resistant towards poisoning and bear a lower cost.[7,11]

Recently, considerable attention has been directed towards catalysts based on mixed metal oxides such as perovskite-type compounds, ABO_3 (A is usually a rare earth and B is a transition metal),[12–16] and ferrospinel-type compounds, AFe_2O_4 (A is a divalent metal).[17–20]

The preparation of catalysts with nanosized particles is the key to an efficient catalytic performance. In nanostructured materials, the interface between nanoparticles and surrounding medium plays a more important role than in the bulk materials. Moreover, the strong curvature of nanoparticles due to their small radius leads to an increased number of the structural defects at the nanoparticle surface, enhancing the surface reactivity. Various synthesis methods have been tested to obtain catalyst materials with superior microstructure, *e.g.* sol–gel,[21] coprecipitation,[22] or combustion reaction.[23] Oliva *et al.*[24] found that the preparation procedure can exert a remarkable influence on the physico-chemical characteristics and catalytic properties of the obtained materials.

In the present work a nonconventional method, sol–gel self-combustion,[25] followed by a thermal treatment, was used to prepare low cost catalysts – perovskite and ferrospinel nanopowders. In this processing technology, the heat generated by a rapid exothermic combustion reaction was used for the synthesis reaction of oxide ceramics. The method requires basic equipment and assures a high purity and homogeneous mixing on the atomic scale. The ceramic materials prepared by sol–gel self-combustion have superior properties with respect to those made by conventional methods and are cheaper to produce. We analyzed comparatively the catalytic performances of the

[a]Alexandru Ioan Cuza University, Integrated Center for Studies in Environmental Science for North-East Region (CERNESIM), 11 Carol I Blvd, 7000506 Iasi, Romania. E-mail: docorneliug@gmail.com; docorneliu@yahoo.com; Tel: +40 730 719855

[b]Alexandru Ioan Cuza University, Faculty of Physics, 11 Carol I Blvd, 7000506 Iasi, Romania

obtained nanopowders utilized in the catalytic flameless combustion of the dilute propane. The influence of various parameters such as chemical composition of the catalysts, crystallite size, surface specific area, reaction temperature and conversion degree of the propane has been investigated. The structural and morphological characterization of the materials was performed using X-ray diffraction (XRD), Scanning Electron Microscopy (SEM), Brunauer–Emmett–Teller (BET) surface area analysis, Energy Dispersive X-ray spectroscopy (EDX) and X-ray photoelectron spectroscopy (XPS).

2. Experimental

2.1. Catalysts preparation and characterization

Five nanograined perovskite powders of nominal compositions: $SrMnO_3$, $SrCoO_3$, $GdAlO_3$, $FeMnO_3$, $La_{0.6}Pb_{0.2}Mg_{0.2}MnO_3$ and four nanograined ferrospinel powders of nominal compositions: $MgFe_2O_4$, $Ni_{0.5}Co_{0.5}Fe_2O_4$, $Ni_{0.5}Co_{0.5}Fe_{1.9}Sc_{0.1}O_4$, $Ni_{0.5}Co_{0.5}Fe_{1.8}Sc_{0.2}O_4$ were prepared by sol–gel self-combustion procedure followed by heat treatment at 900 °C or 1000 °C (depending on the nature of crystalline phase of materials). We used metal nitrates, ammonium hydroxide and polyvinyl alcohol (PVA) as starting materials. A solution containing metal nitrates was mixed with an aqueous solution (10% concentration) of polyvinyl alcohol. A small amount of NH_4OH solution (10% concentration) was dropped to adjust the pH value to about 8. This produced a sol of metal hydroxides and ammonium nitrate. By drying at 100 °C for 12 h, the sol was turned into a dried gel. The dried gel was ignited in a corner and a combustion reaction spontaneously propagated through the whole gel. The obtained powders were calcinated at 500 °C to eliminate the residual organic compounds. Finally, the calcined powders were annealed in air at 900 °C (ferrite powders) or 1000 °C (perovskite powders). Some details on the preparation procedure can be found in earlier publications.[26,27] A total of 9 different samples were synthesized by sol–gel self-combustion, as mentioned in Table 1.

The crystal structure and phase composition of the samples were analyzed by XRD. X-ray diffraction measurements of the powders were performed at room temperature using a PANALYTICAL X' PERT PRO MPD powder diffractometer with Cu-$K_{\alpha 1}$ radiation ($\lambda = 0.15405$ nm). The XRD patterns were registered between 20 and 80° (2θ) at a rate of 2° min^{-1}. The average crystallite size was estimated based on XRD peak broadening, using the Scherrer equation:[28]

$$D_{XRD} = \frac{0.9\lambda}{\beta \cos \theta}, \quad (1)$$

where λ is wavelength of Cu-$K_{\alpha 1}$ radiation, β is the full width at half maximum of the peak, and θ denotes its Bragg diffraction angle. A scanning electron microscope (JEOL-200 CX) was used to visualize the surface morphology of samples. A Quantachrome automated gas adsorption system (Quantachrome Instruments) was used to record N_2 adsorption isotherms at 77 K. The powders were degassed at 300 °C for 1 h before the measurements. The BET specific surface area (S_{BET}) was determined from nitrogen sorption data using the BET equation.[29] The elemental composition of the particle surface was examined with an Energy Dispersive X-ray Spectrometer (EDX) using a voltage of 20 kV. The X-ray (Al-K_α radiation) photoelectron spectroscopy (XPS) was used to distinguish the oxidation state of the cations present on the surfaces.

Table 1 Ferrites and perovskites prepared by sol–gel self-combustion procedure

Sample symbol	Chemical composition	Heat treatment
F1	$MgFe_2O_4$	900 °C, 20 min
F2	$Ni_{0.5}Co_{0.5}Fe_2O_4$	900 °C, 4 h
F3	$Ni_{0.5}Co_{0.5}Fe_{1.9}Sc_{0.1}O_4$	900 °C, 4 h
F4	$Ni_{0.5}Co_{0.5}Fe_{1.8}Sc_{0.2}O_4$	900 °C, 4 h
P1	$SrMnO_3$	1000 °C, 7 h
P2	$SrCoO_3$	1000 °C, 7 h
P3	$FeMnO_3$	1000 °C, 7 h
P4	$GdAlO_3$	1000 °C, 7 h
P5	$La_{0.6}Pb_{0.2}Mg_{0.2}MnO_3$	1000 °C, 2 h

2.2. Catalytic activity measurements

Catalyst activity tests were performed at atmospheric pressure, in a laboratory scale with a flow type set-up (flow rate of 100 cm^3 min^{-1}, propane concentration in air of 1–2‰ and the gas hourly space velocity, GHSV, of 5100 h^{-1}), previously described in ref. 30. The catalyst powder (0.3–0.5 g) was sandwiched between two layers of quartz wool in a quartz tubular microreactor ($\phi = 7$ mm) placed in an electric furnace. The increase of the temperature was made in steps of 50 °C, from 50 to 550 °C. As a result of catalytic combustion, at every predetermined temperature, the gas concentration at the reactor exit was smaller than the inlet gas concentration. The catalytic activity of the nine oxide materials under study was evaluated in terms of propane conversion (to carbon dioxide) rate over these materials:[26,30,31]

$$C = \frac{c_{in} - c_{out}}{c_{in}} \times 100 \ (\%), \quad (2)$$

where c_{in} and c_{out} represent the inlet and outlet propane concentration, respectively, measured with a photoionization detector (PID-TECH) for VOCs, at several temperatures. Data were collected when the flameless catalytic combustion reached a steady state, after about 30 minutes at each temperature. These experiments were repeated decreasing the temperature and similar results were obtained, indicating the stability of ferrites and perovskites over time, and the absence of the deactivation.

3. Results and discussion

3.1. Materials characterization

The XRD patterns at room temperature of the nine powdered samples are shown in Fig. 1. Well defined sharp peaks can be clearly seen in the diffraction patterns and show that as-synthesized materials have a good crystalline quality. Crystalline phases identified by comparing to a known standard, average crystallite size D_{XRD}, derived from XRD data, specific

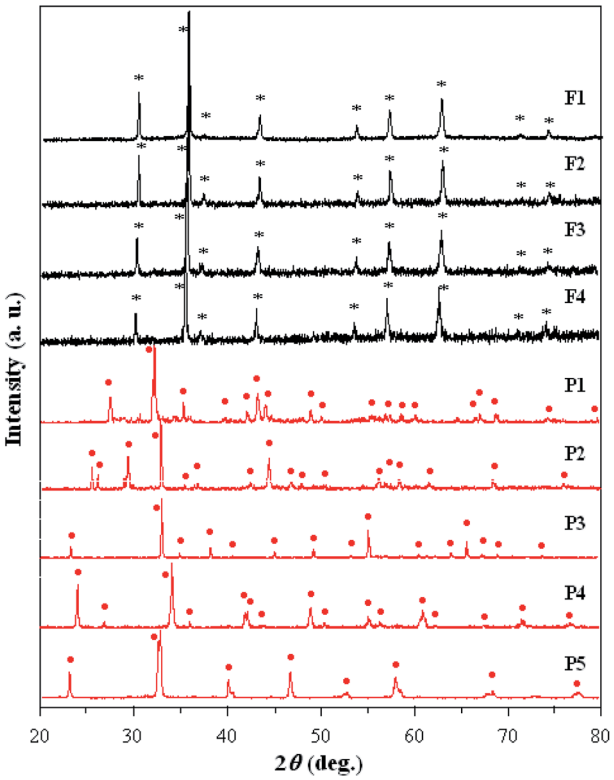

Fig. 1 Powder X-ray diffraction patterns of the investigated samples. (*) – Main phases in studied ferrites; (•) – main phases in studied perovskites.

surface area S_{BET} and pore volume obtained from nitrogen adsorption/desorption isotherms at 77 K, are summarized in Table 2.

On the basis of data presented in Fig. 1 and Table 2, the following remarks can be made:

(a) All samples were indexed as perovskite- or ferrospinel-type structures, without presence of any foreign phase;

(b) Irrespective of phase composition, all materials show nanoscale crystallinity. The average crystallite size, D_{XRD}, was found to be in the range of 26–89 nm. The smallest crystallites were identified in La–Pb–Mg manganite perovskite powder;

(c) The average crystallite size decreased by scandium incorporation in Ni–Co ferrite (F3, F4 samples). This may be due to a structural disorder induced by the larger Sc-ions, which can lead to some delay in the growth of the ferrite crystallites;

(d) The S_{BET} values are smaller for perovskites and ferrites containing only two cations and these results appear to be caused by an effective increase in the degree of crystallinity as a result of the heat treatment. These values are comparable to those reported by other authors,[32] for similar chemical compositions.

The microstructure plays a major role in the performance of a ceramic catalyst and for this reason it was examined by SEM. The surface morphology of the nine materials is shown in SEM micrographies given in Fig. 2. As can be seen, the grains have a rounded shape and the pores are not intragranular. These images also show that samples exhibit similar morphologies, being composed of aggregates of nanograins with irregular shapes and sizes. The images also reveal the presence of large interaggregate pores.

The surface elemental composition of the materials was inspected by EDX analysis. In Fig. 3 the EDX spectra for four catalyst materials are given and their elemental compositions are summarized in Table 3. Each provided composition represents the mean value of three determinations at different points of each sample. One can remark that the chemical composition of the samples is close to the nominal one, *i.e.* the M/M_t (see Table 3) ratios are close to the theoretical values given in parenthesis. This is proof of the homogeneous distribution of the elements in the solids prepared by sol–gel self-combustion technique.

The XPS technique was used to distinguish the oxidation state of the cations present on the surfaces. Among the studied ferrites are presented the XPS spectra of the $Ni_{0.5}Co_{0.5}Fe_{1.8}Sc_{0.2}O_4$ ferrite and among the studied perovskites are presented the XPS spectra of the $La_{0.6}Pb_{0.2}Mg_{0.2}MnO_3$ perovskite. Fig. 4(a) and (b) show the Fe 2p and Sc 2p, respectively, XPS spectra of $Ni_{0.5}Co_{0.5}Fe_{1.8}Sc_{0.2}O_4$ ferrite. However, the analyses of Fe 2p spectra are relatively complex for ferrites. The divalent Fe $2p_{3/2}$ peak at 709.5 eV and the trivalent Fe $2p_{3/2}$ peak at 711.2 eV are respectively associated to satellite peaks at 715.5 eV and 719.0 eV.[19,33–35] In the case of the sample with $Sc_{0.2}$ the observed Fe $2p_{3/2}$ peaks with binding energies (BE) between 711.2 eV and

Table 2 Structure characteristics of investigated samples

Sample symbol	Crystalline phases	D_{XRD} (nm)	S_{BET} ($m^2\ g^{-1}$)	Pore volume ($cm^3\ g^{-1}$)
F1	Cubic spinel	41.8	4.0	0.0060
F2	Cubic spinel	41.7	26.5	0.0053
F3	Cubic spinel	35.2	31.7	0.0072
F4	Cubic spinel	34.8	32.3	0.0089
P1	Hexagonal perovskite	88.9	2.2	0.0010
P2	Hexagonal perovskite	59.9	1.9	0.0030
P3	Cubic perovskite	59.2	3.2	0.0044
P4	Orthorhombic perovskite	39.6	9.8	0.0018
P5	Cubic perovskite	25.8	8.6	0.0021

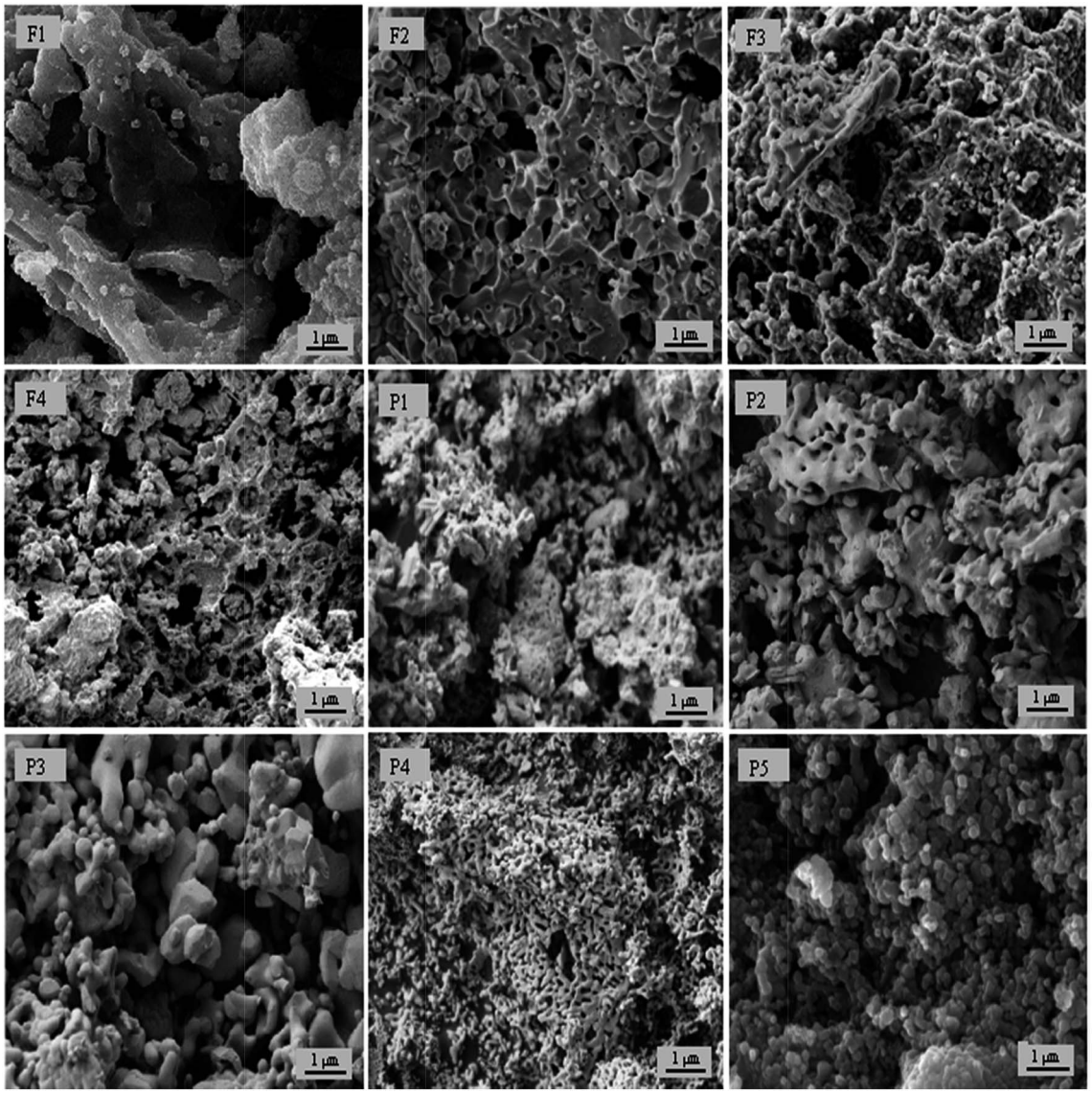

Fig. 2 SEM micrographs of the investigated samples.

713.0 eV, and the associated satellite at around 716.3 eV and 720.0 eV (Fig. 4a), confirm the predominance of Fe^{3+} and a small fraction of Fe^{2+} present on the sample surface.[19,35,36] The observed BE shifts can be attributed to the different surroundings of the Fe^{3+} ions in the A and B sites and of the Sc^{3+} ions (Fig. 4b) in the B (octahedral) site within the ferrite structure.

Fig. 5(a) and (b) show the Mn 2p and La 3d, respectively, XPS spectra of $La_{0.6}Pb_{0.2}Mg_{0.2}MnO_3$ perovskite. The La 3d level is characterised by a double peak for each components (La $3d_{3/2}$ and La $3d_{5/2}$). The Mn 2p peak was decomposed in 2 components. The full width at half maximum (FWHM) of which were imposed to be equal: a component at 653.6 attributed to Mn $2p_{1/2}$ and a component at 641.9 attributed to Mn $2p_{3/2}$.[37] The binding energies of the elements present in the parent perovskite ($LaMnO_3$) reported by Arendt *et al.*[38] are the following: 641.9 eV for Mn $2p_{3/2}$, 834.0 eV for La $3d_{5/2}$, 851.0 eV for La $3d_{3/2}$, 529.1 eV for O(I) 1s and 530.6 eV for O(II) 1s. The binding energies of the elements present in the $La_{0.67}Pb_{0.33}MnO_3$ reported by Kowalik *et al.*[39] are the following: 641.1 eV for Mn^{3+} $2p_{3/2}$, 643.2 eV for Mn^{4+} $2p_{3/2}$, 645.7 eV for Pb $4p_{3/2}$ and 2.02 for the Mn^{3+}/Mn^{4+} ratio. The binding energies of the perovskite catalyst used by us ($La_{0.6}Pb_{0.2}Mg_{0.2}MnO_3$) are characterised by values very close to those reported above: 641.5 eV for Mn^{3+} $2p_{3/2}$, 643.1 eV for Mn^{4+} $2p_{3/2}$, 644.9 eV for Pb $4p_{3/2}$, 653.1 eV for Mn^{3+} $2p_{1/2}$, 654.5 eV for Mn^{4+} $2p_{1/2}$, 834.2 eV for La $3d_{5/2}$ (838.4 eV for satellite), 850.9 eV for La $3d_{3/2}$ (855.2 eV for satellite) and 1.40 for the Mn^{3+}/Mn^{4+} ratio.

3.2. Catalytic activity

The catalytic combustion tests of propane over the nine catalyst samples were performed as a function of temperature. Propane oxidation reaction on the catalyst surface takes place according to a radical mechanism consisting of several stages. Global

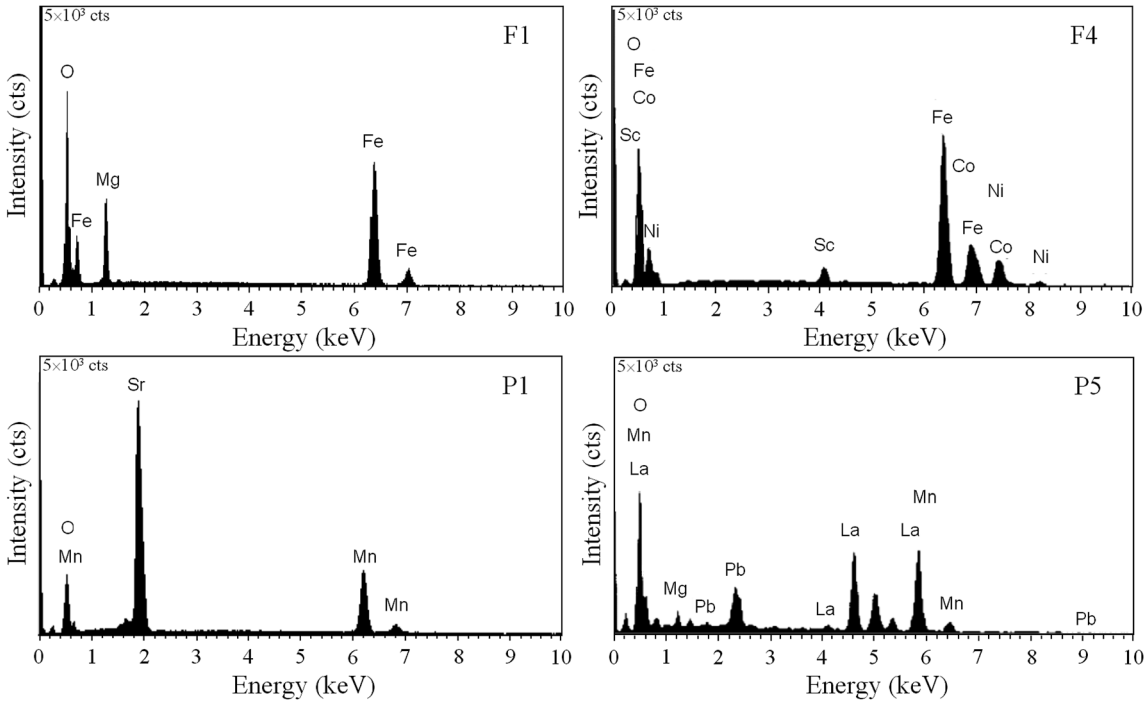

Fig. 3 EDX spectra for $MgFe_2O_4$ (F1), $Ni_{0.5}Co_{0.5}Fe_{1.8}Sc_{0.2}O_4$ (F4), $SrMnO_3$ (P1) and $La_{0.6}Pb_{0.2}Mg_{0.2}MnO_3$ (P5).

oxidation reaction of propane, summing all stages of this mechanism, will be as follows:

$$C_3H_8 + 5O_2 = 3CO_2 + 4H_2O. \quad (3)$$

In one of these stages catalyst contribution occurs, which will speed up the process of combustion through its intervention from time to time, until all residues of hydrocarbon species are consumed, finally yielding CO_2 and H_2O.

Several repetitions of tests led to similar results, thus indicating reproducibility of actual experimental data. Some of these results were published in previous articles.[30,40]

Results showing the temperature dependence of propane conversion in its combustion reaction over all catalysts are presented in Fig. 6. The catalysts exhibited substantial differences in catalytic activity, in the temperature range of 200–400 °C. The conversion data in Fig. 6 suggest a significant influence of the chemical composition of the catalyst on the propane conversion at different temperatures. It should be noted that no catalytic activity was observed at temperatures below 100 °C. Moreover, the catalytic activity of $SrCoO_3$, $GdAlO_3$ and $FeMnO_3$ in propane combustion reaction started at temperatures over 200 °C and temperatures above that level had rather limited influence on their activity.

Among the nine catalysts, the $La_{0.6}Pb_{0.2}Mg_{0.2}MnO_3$ perovskite showed the highest propane combustion activity at low temperatures (below 350 °C). This catalyst was able to convert 50% of propane at temperature of 224 °C and 90% at 320 °C. The high improved catalytic activity may be attributed to the very small crystallites (26 nm), as well as to the oxygen vacancies generated by the presence of both manganese ions with variable valence,[41,42] fact confirmed by us by analyzing XPS spectra in Fig. 5a. The partial substitution of La^{3+} ions by lower valence ions (as Pb^{2+}–Mg^{2+}) in $LaMnO_3$ perovskite leads to the oxidation

Table 3 EDX analysis of some metal oxide catalysts[a,b]

$MgFe_2O_4$	$GdAlO_3$	$SrMnO_3$	$SrCoO_3$	$Ni_{0.5}Co_{0.5}Fe_{1.8}Sc_{0.2}O_4$	$La_{0.6}Pb_{0.2}Mg_{0.2}MnO_3$
O (at%) 54.44	O (at%) 64.18	O (at%) 62.11	O (at%) 60.80	O (at%) 49.39	O (at%) 63.85
Mg (at%) 15.08	Gd (at%) 17.82	Sr (at%) 21.50	Sr (at%) 20.84	Ni (at%) 8.09	La (at%) 11.61
Fe (at%) 30.48	Al (at%) 18.00	Mn (at%) 16.39	Co (at%) 18.36	Co (at%) 9.82	Mn (at%) 18.04
Mg/Mt 0.33 (0.33)	Gd/Mt 0.5 (05)	Sr/Mt 0.56 (0.5)	Sr/Mt 0.53 (0.5)	Sc (at%) 3.34	Mg (at%) 4.02
Fe/Mt 0.67 (0.66)	Al/Mt 0.5 (0.5)	Mn/Mt 0.44 (0.5)	Co/Mt 0.47 (0.5)	Fe (at%) 29.36	Pb (at%) 2.47
				Ni/Mt 0.16 (0.17)	La/Mt 0.3 2 (0.3)
				Co/Mt 0.19 (0.17)	Mn/Mt 0.50 (0.5)
				Sc/Mt 0.07 (0.07)	Mg/Mt 0.11(0.1)
				Fe/Mt 0.58 (0.60)	Pb/Mt 0.07 (0.1)

[a] M_t is total amount of metallic composition on the surface. [b] In parenthesis are given theoretical values.

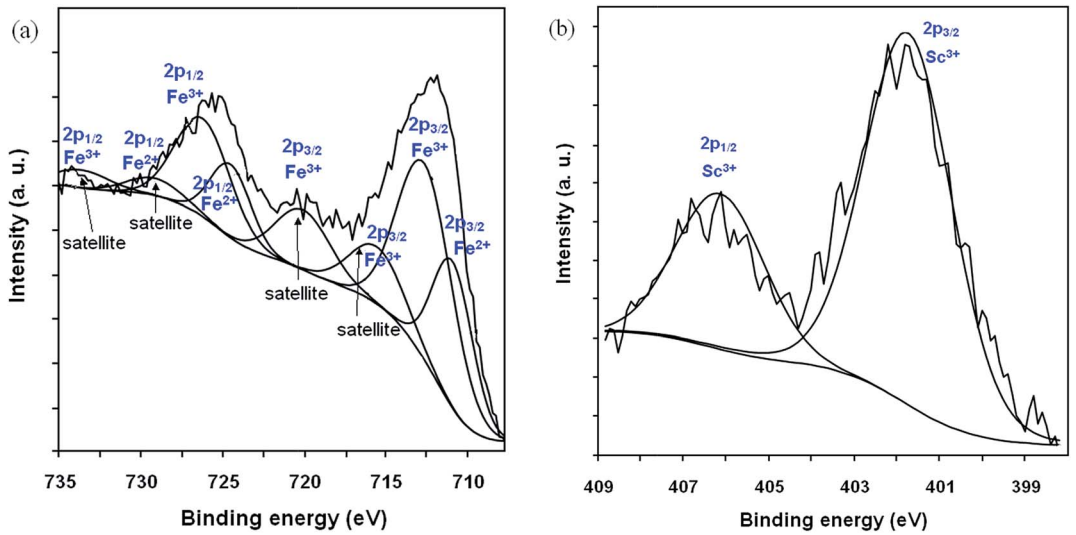

Fig. 4 XPS spectra of the Fe 2p (a) and Sc 2p (b) of the $Ni_{0.5}Co_{0.5}Sc_{0.2}Fe_{1.8}O_4$ powder.

of Mn^{3+} to Mn^{4+} and the formation of oxygen vacancies (active sites for oxygen adsorption).[41,42] The oxygen vacancies are essential for the adsorption/dissociation of oxygen molecules during the catalytic oxidation reaction and strongly affect the catalytic activity of the catalyst. More oxygen vacancies involve a larger density of adsorbed oxygen species (O^-, O_2^-, O^{2-}), weakly anchored on the catalyst surface, which favors the VOC oxidation. The larger the number of oxygen ions adsorbed, the faster the gas oxidation reaction would be.

From Fig. 6 one can also remark that $SrMnO_3$ perovskite and $Ni_{0.5}Co_{0.5}Fe_{1.8}Sc_{0.2}O_4$ ferrite show similar catalytic activities in the temperature range 150–350 °C, even if these catalysts display different compositions and crystallographic structures. Both catalysts can convert 50% of propane in CO_2 and H_2O at the same low temperature, of about 240 °C. Moreover, at 350 °C a high conversion degree of propane, of 88–89%, was obtained over the two catalysts.

Even at low conversions, CO was not observed among the final products and this indicates that propane was completely converted to CO_2 and H_2O.

The less efficient catalytic performance in propane conversion was registered for $SrCoO_3$ (32% conversion rate at 500 °C) and $FeMnO_3$ (13% conversion rate at 500 °C), although our previous work[40] showed that these perovskites exhibit high catalytic activity towards acetone conversion. The reasons for such a selective catalytic activity of $SrCoO_3$ and $FeMnO_3$ are not yet clear. A dependence of activity on the surface area was not found. Other factors, such as structural defects or oxygen mobility, are likely to control the catalytic activity of oxide catalysts.

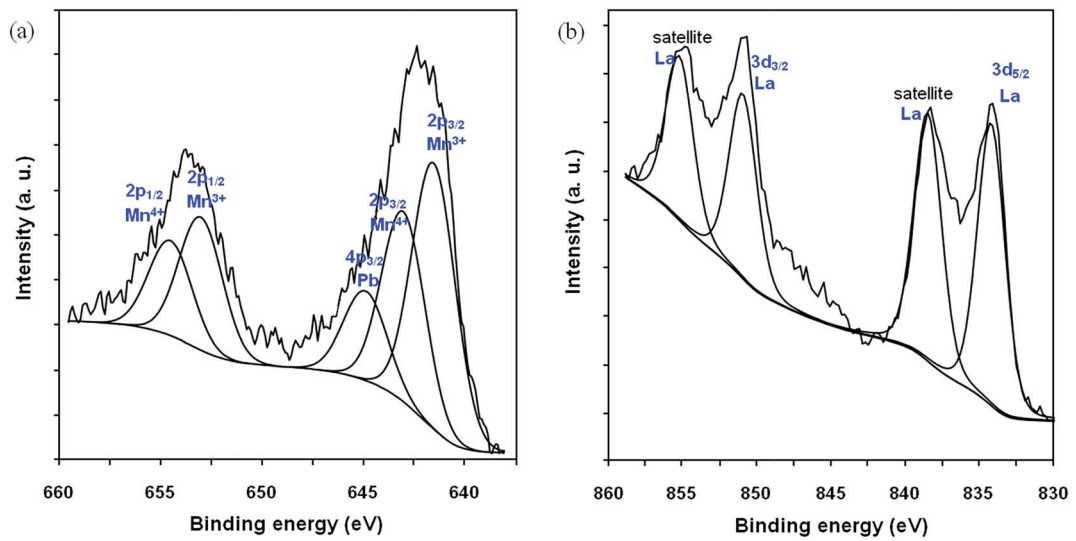

Fig. 5 XPS spectra of the Mn 2p and Pb 4p (a) and La 2p (b) of the $La_{0.6}Pb_{0.2}Mg_{0.2}MnO_3$ powder.

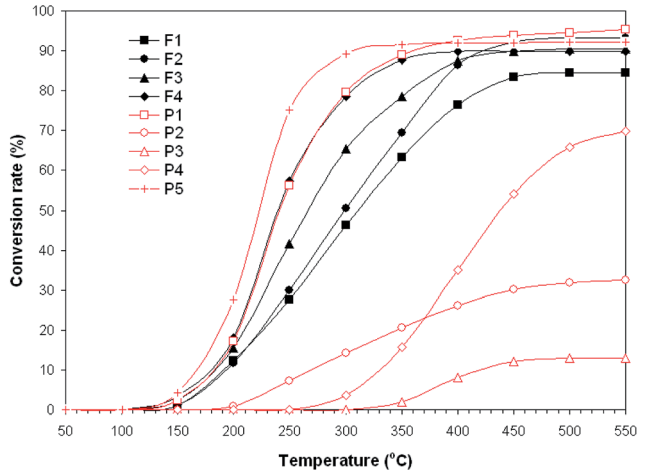

Fig. 6 Conversion rate *versus* temperature in the catalytic combustion of propane over the nine catalyst samples: $MgFe_2O_4$ (F1), $Ni_{0.5}Co_{0.5}Fe_2O_4$ (F2), $Ni_{0.5}Co_{0.5}Fe_{1.9}Sc_{0.1}O_4$ (F3), $Ni_{0.5}Co_{0.5}Fe_{1.8}Sc_{0.2}O_4$ (F4), $SrMnO_3$ (P1), $SrCoO_3$ (P2), $FeMnO_3$ (P3), $GdAlO_3$ (P4) and $La_{0.6}Pb_{0.2}Mg_{0.2}MnO_3$ (P5).

It is interesting to note, from the results presented in Fig. 6, that the $La_{0.6}Pb_{0.2}Mg_{0.2}MnO_3$ catalyst, which shows the highest propane combustion activity at low temperatures, is a pure cubic perovskite as is the $FeMnO_3$ catalyst, which exhibits very low propane combustion activity. This suggests that the high catalytic activity of the first may be related to the presence of the structural defects (oxygen vacancies) created by the decreasing crystallite size (Table 2).

The main indicator of catalytic activity of a given catalyst is typically temperature T_{50} – the temperature required for 50% conversion of a gas. At T_{50} temperature the catalytic activity is sufficiently high and the interactions between catalyst surface and reactants are intense. The lower this parameter is, the higher the activity of the catalyst is. In Table 4 the values of T_{50} and T_{90} (the temperature required for 90% propane conversion) for all catalysts are listed. The T_{50} and T_{90} temperatures for the most active catalyst, $La_{0.6}Pb_{0.2}Mg_{0.2}MnO_3$, are much lower than those for the other catalysts. As present studies revealed, the degree of propane conversion for $SrCoO_3$ and $FeMnO_3$ perovskite catalysts is smaller than 50%. The catalytic performance of $La_{0.6}Pb_{0.2}Mg_{0.2}MnO_3$ catalyst in combustion reaction of propane is comparable to that of the Pt/Al_2O_3 noble metal catalyst, which could achieve 50% conversion of propane at 325 °C and 90% at 400 °C.[43]

It can be assumed that the catalytic combustion of propane vapor takes place in the presence of excess oxygen. The apparent activation energies (E_a) for the catalytic reactions were calculated by means of the Arrhenius-type plot of the natural logarithm of the reaction rate (k) at very low conversion, below 20%, *versus* inverse temperature ($1/T$).[44–47] The Arrhenius equation can be given in the form:[44,48]

$$k = A \exp(-E_a/RT) \quad (4)$$

where k, A, R and E_a are the reaction rate, preexponential factor, gas constant and apparent activation energy, respectively.

Table 4 also includes the values of the kinetic parameters (apparent activation energy, E_a, and reaction rate, k) for propane oxidation over the nine catalysts. Reaction rates are normalized to the BET surface area, in order to compare the specific catalytic activities of the catalysts. One can observe that the normalized reaction rate changes from 3.8×10^{-2} μmol (s^{-1} m^{-2}) to 11×10^{-2} μmol (s^{-1} m^{-2}), in dependence of catalyst composition. The highest value of the reaction rate [11×10^{-2} μmol (s^{-1} m^{-2})] was obtained for propane combustion over $La_{0.6}Pb_{0.2}Mg_{0.2}MnO_3$ catalyst, which proved the best propane conversion rate, of 92%, at 350 °C (see Fig. 6).

In Table 4 one can observe the wide variation in determined activation energies from 28 kJ mol^{-1} to 85 kJ mol^{-1}. The smallest value (28 kJ mol^{-1}) of the activation energy was registered for $La_{0.6}Pb_{0.2}Mg_{0.2}MnO_3$ catalyst, for which the reaction rate was the highest. The differences observed between the activation energies of the nine catalysts allow one to speculate that the nature of the catalytic sites differs from one catalyst to another. We mention that the values of the kinetic parameters provided here are comparable to those presented by other authors for other oxides and VOCs.[49,50]

The present study suggests that $La_{0.6}Pb_{0.2}Mg_{0.2}MnO_3$ perovskite catalyst can be a promising candidate to substitute highly expensive noble metal catalysts used in propane combustion. Further investigations of other ferrite and perovskite compositions are required, in order to find new catalyst compositions with better performances.

Table 4 T_{50}, T_{90}, propane conversion at 400 °C and kinetic parameters

Symbol	T_{50} (°C)	T_{90} (°C)	$Conv_{400}$ (%)	Reaction rate[a] (μmol s^{-1} m^2)	Activation energy[b] (kJ mol^{-1})
F1	311	—	76	8.14×10^{-2}	75
F2	300	418	86	4.57×10^{-2}	82
F3	267	432	88	4.66×10^{-2}	65
F4	240	380	90	5.53×10^{-2}	50
P1	240	400	90	9.8×10^{-2}	31
P2	—	—	26	3.8×10^{-2}	48
P3	—	—	8	6.1×10^{-2}	80
P4	438	—	35	7.8×10^{-2}	71
P5	224	320	92	11.0×10^{-2}	28

[a] Reaction rate at low conversion per unit surface area of catalyst. [b] Apparent activation energy for low conversions.

4. Conclusions

Composite oxides catalysts (ferrites: $MgFe_2O_4$, $Ni_{0.5}Co_{0.5}Fe_2O_4$, $Ni_{0.5}Co_{0.5}Fe_{1.9}Sc_{0.1}O_4$, $Ni_{0.5}Co_{0.5}Fe_{1.8}Sc_{0.2}O_4$ and perovskites: $SrMnO_3$, $SrCoO_3$, $GdAlO_3$, $FeMnO_3$, $La_{0.6}Pb_{0.2}Mg_{0.2}MnO_3$) for propane combustion can be obtained by sol–gel self-combustion technique, followed by heat treatment. Among the nine studied compounds, $La_{0.6}Pb_{0.2}Mg_{0.2}MnO_3$ perovskite was found to exhibit the best catalytic performance with respect to propane combustion at low temperatures: a 92% conversion rate at 350 °C. This perovskite catalyst is a promising candidate to substitute expensive noble metal catalysts in propane combustion.

References

1 Z. Fan, P. Lioy, K. Veschler, N. Fiedler, H. Kipen and J. Zhang, *Environ. Sci. Technol.*, 2003, **37**, 1811–1821.
2 W. B. Li, W. B. Chu, M. Zhuang and J. Hua, *Catal. Today*, 2004, **93–95**, 205–209.
3 W. B. Li, J. X. Wang and H. Gong, *Catal. Today*, 2009, **148**, 81–87.
4 K. Everaert and J. Baeyens, *J. Hazard. Mater.*, 2004, **109**, 113–139.
5 H. G. Ahn, B. M. Choi and D. J. Lee, *J. Nanosci. Nanotechnol.*, 2006, **6**, 3599–3603.
6 L. van de Beld, M. C. van der Ven and K. R. Westerterp, *Chem. Eng. Process.*, 1995, **34**, 469–478.
7 S. C. Kim and W. G. Shim, *Appl. Catal., B*, 2010, **98**, 180–185.
8 A. K. Sinha and K. Suzuki, *Angew. Chem., Int. Ed.*, 2005, **44**, 271–273.
9 D. Kim and S. Ihm, *Environ. Sci. Technol.*, 2001, **35**, 222–226.
10 K. Jirátová, J. Mikulová, J. Klempa, T. Grygar, Z. Bastl and F. Kovanda, *Appl. Catal., A*, 2009, **361**, 106–116.
11 M. R. Morales, B. P. Barbero and L. E. Cadús, *Fuel*, 2008, **87**, 1177–1186.
12 L. G. Tejuca, J. L. G. Fierro and J. M. O. Tascon, *Adv. Catal.*, 1989, **36**, 327–328.
13 N. Yamazoe and Y. Teraoka, *Catal. Today*, 1990, **8**, 175–199.
14 T. Seiyama, *Catal. Rev.: Sci. Eng.*, 1992, **34**, 281–300.
15 A. Musialiak-Piotrowska and K. Syczewska, *Catal. Today*, 2000, **59**, 269–278.
16 M. A. Pena and J. L. G. Fierro, *Chem. Rev.*, 2001, **101**, 1981–2018.
17 A. Urda, A. Herraïz, A. Rédey and I. C. Marcu, *Catal. Commun.*, 2009, **10**, 1651–1655.
18 M. Florea, M. Alifanti, V. I. Parvulescu, D. Mihaila-Tarabasanu, L. Diamandescu, M. Feder, C. Negrila and L. Frunza, *Catal. Today*, 2009, **14**, 361–366.
19 A. S. Albuquerque, M. V. C. Tolentino, J. D. Alrdisson, F. C. C. Moura, R. de Mendonça and W. A. A. Macedo, *Ceram. Int.*, 2012, **38**, 2225–2231.
20 C. C. Ramankutty and S. Sugunan, *Appl. Catal., A*, 2001, **218**, 39–51.
21 N. Chu, X. Wang, Y. Liu, H. Jin, Q. Wu, L. Li, Z. Wang and H. Ge, *J. Alloys Compd.*, 2009, **470**, 438–442.
22 A. B. Gadkari, T. J. Shinde and P. N. Vasambekar, *Mater. Chem. Phys.*, 2009, **114**, 505–510.
23 A. C. F. M. Costa, R. T. Lula, R. H. G. A. Kiminami, L. F. V. Gama, A. A. de Jesus and H. M. C. Andrade, *J. Mater. Sci.*, 2006, **41**, 4871–4875.
24 C. Oliva, L. Bonoldi, S. Cappelli, L. Fabbrini, I. Rossetti and L. Forni, *J. Mol. Catal. A: Chem.*, 2005, **226**, 33–40.
25 P. D. Popa, N. Rezlescu and G. Iacob, A new procedure for preparing ferrite powders, Romanian Patent No. 121300, OSIM, Bucharest, 2008.
26 N. Rezlescu, E. Rezlescu, P. D. Popa, E. Popovici, C. Doroftei and M. Ignat, *Mater. Chem. Phys.*, 2013, **137**, 922–927.
27 C. Doroftei, P. D. Popa, F. Iacomi and L. Leontie, *Sens. Actuators, B*, 2014, **191**, 239–245.
28 B. D. Cullity and R. S. Stock, *Elements of X-Ray Diffraction*, Prentice Hall, New Jersey, 3rd edn, 2001.
29 S. Lowell, J. E. Shields, M. A. Thomas and M. Thommes, Characterization of Porous Solids and Powders: Surface Area, *Pore Size and Density*, Kluwer Academic Publishers, Dordrecht-Boston-London, 2004.
30 N. Rezlescu, E. Rezlescu, P. D. Popa, C. Doroftei and M. Ignat, *Ceram. Int.*, 2015, **41**, 4430–4437.
31 C. Doroftei, P. D. Popa, E. Rezlescu and N. Rezlescu, *J. Alloys Compd.*, 2014, **584**, 195–198.
32 Y. I. Pyatnitskii, A. I. Bostan, L. N. Raevskaza, S. A. Nedil'ko, A. G. Dzyaz'ko and E. G. Zen'kovich, *Theor. Exp. Chem.*, 2005, **41**, 117–121.
33 V. K. Mittal, P. Chandramohan, S. Bera, M. P. Srinivasan, S. Velmurugan and S. V. Narasimhan, *Solid State Commun.*, 2006, **137**, 6–10.
34 T. Yamashita and P. A. Hayes, *Appl. Surf. Sci.*, 2008, **254**, 2441–2449.
35 H. J. Lee, M. H. Park, Y. J. Kim, C. S. Hwang, J. H. Kim, H. Funakubo and H. Ishiwara, *J. Appl. Phys.*, 2011, **110**, 074111–074118.
36 N. S. McIntyre and D. G. Zetaruk, *Anal. Chem.*, 1977, **49**, 1521–1529.
37 J. F. Moulder, W. F. Stickel, P. E. Sobol and K. D. Bomben, in *Handbook of X-ray Photoelectron Spectroscopy*, ed. J. Chastain, 1992.
38 E. Arendt, A. Maione, A. Klisinska, O. Sanz, M. Montes, S. Suarez, J. Blanco and P. Ruiz, *Appl. Catal., A*, 2008, **339**, 1–14.
39 M. Kowalik, R. Zalecki and A. Kolodziejczyk, *Acta Phys. Pol., A*, 2010, **117**, 227–280.
40 N. Rezlescu, E. Rezlescu, P. D. Popa, C. Doroftei and M. Ignat, *Composites, Part B*, 2014, **60**, 515–522.
41 A. Kaddouri, P. Gelin and N. Dupont, *Catal. Commun.*, 2009, **10**, 1085–1089.
42 R. M. G. de la Cruz, H. Falcon, M. A. Pena and J. I. G. Fierro, *Appl. Catal., B*, 2001, **33**, 45–55.
43 R. Burch, E. Halpin, M. Hayes, K. Ruth and J. A. Sullivan, *Appl. Catal., B*, 1998, **19**, 199–207.
44 L. Kundakovic and M. F. Stephanopoulos, *J. Catal.*, 1998, **179**, 203–221.
45 H. G. El-Shobaky and M. M. Mokhtar, *Appl. Surf. Sci.*, 2007, **253**, 9407–9413.

46 R. C. Everson, L. N. Mulay, O. P. Mahajan and P. L. Walker, *J. Chem. Technol. Biotechnol.*, 1979, **29**, 1–7.
47 V. G. Milt, M. A. Ulla and E. A. Lombardo, *Catal. Lett.*, 2000, **65**, 67–73.
48 H. Arandiyan, H. Dai, K. Ji, H. Sun and J. Li, *ACS Catal.*, 2015, **5**, 1781–1793.
49 V. G. Milt, R. Spretz, M. A. Ulla and E. A. Lombardo, *Catal. Lett.*, 1996, **42**, 57–63.
50 K. S. Song, D. Klvana and J. Kirchnerova, *Appl. Catal., A*, 2001, **213**, 113–121.